Electronic Supplementary Information:

Topotactic elimination of water across a C-C ligand bond in a dense 3-D metal-organic framework

Hamish H.-M. Yeung, [a,b] Monica Kosa,[c] John M. Griffin,[d] Clare P. Grey,[d] Dan T. Major[c] and Anthony K. Cheetham*[a]

[a] *Department of Materials Science and Metallurgy, Cambridge University, Charles Babbage Road, Cambridge, UK, CB3 0FS.*
[b] *International Center for Young Scientists, WPI Center for Materials Nanoarchitectonics, National Institute of Materials Science, 1-1 Namiki, Tsukuba, Ibaraki, 305-0044, Japan.*
[c] *Department of Chemistry, Faculty of Exact Sciences and the Lise Meitner-Minerva Center of Computational Quantum Chemistry, Bar Ilan University, Ramat Gan, Israel, IL-52900.*
[d] *Department of Chemistry, Cambridge University, Lensfield Road, Cambridge, UK, CB2 1EW.*
** Corresponding author, email akc30@cam.ac.uk.*

S1. Experimental Details.

All reagents were bought and used as received: L-malic acid (99 %, Fisher), lithium acetate dihydrate (98 %, Acros), lithium hydroxide monohydrate (reagent grade, Fisher), fumaric acid (99 %, Sigma), absolute ethanol and deionised water (both analytical reagent grade, Fisher).

Single crystals of lithium l-malate [Li_2(L-$C_4H_4O_5$)], **1**, were synthesised as described previously.[1] L-malic acid (1 mmol) was dissolved in water:ethanol (1:9, 5 ml), lithium acetate dihydrate (2 mmol) was dissolved in water ethanol (1:4, 5 ml) and the solutions combined in a PTFE-capped borosilicate glass vial at 70 °C. After 8 days, colourless blocks had formed on the vial sides. The product, Li_2(mal) (56 mg, 38 %), was filtered, washed in methanol and dried in air at 70 °C overnight. Elemental analysis: C 32.99 %, H 2.64 %, N 0.0 % (calculated for $C_4H_4Li_2O_5$: C 32.92 %, H 2.76 %, N 0.0 %).

Single crystals of **1** (100 mg), prepared using the procedure described above, were heated to 320 °C in a box furnace for 22 hours, before cooling slowly to room temperature with the furnace closed. Upon examination, the original material had cracked into smaller crystals (87.3 mg), but the crystal quality was retained. Suitable crystals were selected for single crystal X-ray diffraction studies. Similar heat treatments were performed at different temperatures and times, yielding single crystals with different ligand ratios, which were used for single crystal X-ray diffraction.

Single crystals of lithium fumarate, **3**, were synthesized by dissolving fumaric acid (0.5 mmol) and lithium hydroxide monohydrate (1.0 mmol) in water (1 ml). Ethanol (3 ml) was added, resulting in a cloudy suspension, which became clear upon addition of the minimal amount of water. The solution was placed in a PTFE-lined stainless steel autoclave and heated at 180 °C for four days, then cooled to room temperature. Suitable colourless blocky crystals were separated from the discoloured mother liquor for single crystal X-ray diffraction analysis. A bulk sample for further analyses was synthesized as follows: fumaric acid (5.0 mmol) and lithium hydroxide monohydrate (10.0 mmol) were dissolved in water (5 ml) and the resulting solution was filtered through cotton wool into a 12ml borosilicate glass vial. The lid was opened slightly to allow slow evaporation of the solvent and the vial was heated at 60 °C for 16 days. The white crystalline precipitate (450 mg, 70 %) was separated from the mother liquor (pH 6) by filtration, washed with water and dried in air at 60 °C overnight. Elemental analysis: C 37.51 %, H 1.49 %, N 0.0 % (calculated for $Li_2C_4H_2O_4$: C 37.55 %, H 1.58 %, N 0.0 %). The Fourier-transform infrared spectrum contained absorption bands at ν_{max} (cm^{-1}) = 3063, 2980 and 2945 (C-H stretches), 1591 and 1568 (CO_2^-, antisymmetric stretch), 1400 (CO_2^-, symmetric stretch), 1213, 978 (*trans*-HC=CH out of plane), 810, 681 and 584 (Li-O and fingerprint region).

Laboratory crystal structure determination by X-ray diffraction was performed on a Oxford Diffraction Gemini E Ultra diffractometer equipped with dual source Cu radiation (λ = 1.54184 Å, operating at 40 kV and 40 mA with confocal mirrors to increase flux) and Mo radiation (λ = 0.7107 Å, operating at 50 kV and 40 mA). Data were collected at 120 K using ω scans and the mean detector area resolution was 10.4 pixels mm^{-1}. Data collection, cell determination and refinement, intensity integration and face indexation were performed using CrysAlisPro software.[2] Structures were solved by direct methods and full matrix least-squares refinements against $|F^2|$ were carried out using the SHELXTL-PLUS[3] package of programs within the WinGX interface.[4] All non-hydrogen atoms were refined anisotropically; hydrogen atoms were then inserted using a riding model and refined with isotropic displacement parameters constrained to 1.2 and 1.5 times those of their adjacent carbon (non-methyl) and oxygen and methyl carbon atoms, respectively. EADP constraints and DFIX restraints were used on the central malate ligand carbon atoms to

maintain a stable, chemically-sensible refinement. Visualization of structures was carried out using Diamond.[5]

^{13}C and ^{1}H nuclear magnetic resonance spectra were recorded on a Bruker DRX-500 (500 MHz) spectrometer by Cambridge University Department of Chemistry NMR Service. Deuterated water was used as a solvent and internal deuterium lock and proton decoupling was used for ^{13}C spectra. Chemical shifts are relative to tetramethylsilane (δ_H = 0.00 ppm).

Fourier-transform infrared spectroscopy was carried out using a Bruker Tensor 27 Infrared Spectrometer with a diamond attenuated total reflectance (ATR) attachment in absorbance mode. Multiple spectra were recorded in the range 4000-500 cm^{-1} and subsequently averaged.

13C solid-state NMR experiments were performed using a Bruker Avance spectrometer operating at a magnetic field strengths of 9.4 T, corresponding to a 1H Larmor frequency of 400 MHz. Samples were packed into 4-mm MAS rotors and rotated at a MAS rate of 12.5 kHz. 13C transverse magnetisation was obtained by ramped cross polarisation (CP) from 1H with a contact time of 1 ms. Two-pulse phase modulation (TPPM) 1H decoupling was applied during acquisition. A recycle interval of 10 s was used. The spectra shown are the result of coadding 256 and 6144 transients for compounds **1** and **2**, respectively. 13C chemical shifts are given relative to tetramethyl silane at 0 ppm. DFT calculations for the prediction of spectra were performed using CASTEP, a periodic planewave pseudopotential code which utilizes the GIPAW formalism to reconstruct the all-electron wave function in a magnetic field. The generalized gradient approximation (GGA) PBE functional was used and the core-valence interactions described by ultrasoft pseudopotentials. Integrals over the Brillouin zone were performed using a Monkhurst-Pack grid with a k-point spacing of 0.05 Å-1. Wavefunctions were expanded in planewaves with a kinetic energy smaller than the cutoff energy, typically ~680 eV. Structural parameters (the unit cell and atomic positions) were obtained from diffraction data. Geometry optimization was also performed within CASTEP, with the unit cell size and shape remaining fixed.

For main DFT calculations, the geometries and cell parameters of each structure were fully optimized with the VASP 5.2.12 program,[6–9] using the projector augmented wave (PAW)[10,11] pseudo potentials (PP), a 500 eV plane wave energy cutoff in conjunction with the PBE[12] functional. The local dispersion corrections, termed DFT+D2[13] and DFT+D3[14] were used. The ZPE correction was computed by the procedure recently used by us,[15,16] Rivera *et al.*[17] and Wang *et al.*,[18] for example, based on the vibrational frequencies in the harmonic approximation. The vibrational frequencies, derived from the dynamical matrix (as implemented in the VASP 5.2.12 program), were computed with the 600 eV plane wave energy cutoff, using the IBRION = 6 keyword (in VASP 5.2.12 program) and the step size (used to compute the derivative, finite differences) tag POTIM = 0.015. To assess the accuracy of the forces and the step size, for the numerical derivative, we tested the vibrational frequencies using the ADDGRID = .TRUE. and POTIM = 0.01 tags. These refined test calculations were performed for the 3 systems: Li_2(L-malate) (**1**), Li_2(fumarate) (**2(1)**) and Li_2(fumarate) (**3**) and are shown in Table S5.

Thermogravimetric analysis was performed using a TA Instruments Q500 TGA instrument with an air flow of 60 ml min^{-1} at a heating rate of 10 °C min^{-1}, from room temperature to 700 °C using 9 - 13 mg samples.

Variable temperature X-ray diffraction data were collected on a Bruker D8 Advance theta/theta (fixed sample) diffractometer with a VANTEC-1 detector and Goeble mirror for parallel beam optics, in reflection mode using Cu Kα radiation (λ = 1.5418 Å). The ground sample was held on a glass alumina plate inside an MRI heating stage under slow air flow. Scans were taken over an angular range of 6° - 60° (2θ) with step size 0.022° at 2.5 s/step. Scans were taken at 30°C, 70 °C, 110°C, 150°C and at 10°C intervals up to 310°C, with a heating rate of 0.25 °C/s and 600s delay between steps. Data was analysed using LeBail fitting in GSAS-II, including ~85 Pawley peaks, 5-6 Chebyshev background cooefficients and 6-12 background peaks (corundum from the sample holder and Li_2CO_3 decomposition product). The data was cut off below 10°2θ and above d_{min} = 1.54 Å to include only significant data in the refinement. Peaks were modeled using a pseudo-Voigt peak shape, allowing U, V, W and X to refine freely in the latter cycles. Sample displacement and the cell parameters *a* and *c* were refined (space group *R*3). Due to difficulty modeling the peak shapes (likely to be caused by the complex sample structure – disorder, multiple phases with similar cell parameters, inhomogeneity in domain structure etc.), peak intensities could not be reliably obtained. Therefore, Rietveld refinement could not be performed to obtain atomic positions etc. It should be noted that the model fit becomes progressively worse with temperature above 250 °C, where some peak positions, particularly at higher angles, seem to be badly aligned (see Fig. S6-9). The temperature measured in the VT diffraction cell, $T_{diffraction}$, appears lower than expected from other measurement techniques, possibly due to the distance between the thermocouple and the sample within the cell.

Table S1. Single crystal X-ray diffraction data for 2(*x*) after different heat treatments of 1 (*x* determined by refining fractional occupancies against single crystal data), and 3.

	Li_2(L-mal)$_{0.43}$(fum)$_{0.57}$	Li_2(L-mal)$_{0.23}$(fum)$_{0.77}$	Li_2(L-mal)$_{0.20}$(fum)$_{0.80}$	Li_2(fumarate), **3**
Heat treatment	320 °C, 10 hours	320 °C, 22 hours	350 °C, 20 hours	n/a
crystal size (mm)	0.2 × 0.1 × 0.05	0.2 × 0.2 × 0.2	0.9 × 0.8 × 0.6	0.9 × 0.35 × 0.05
crystal system	Trigonal	Trigonal	Trigonal	Triclinic
space group	*R* 3	*R* 3	*R* 3	*P* -1
T (K)	119.95 (10)	120.00(10)	120.00(10)	120.00(10)
a (Å)	11.8093(10)	11.7600(6)	11.7253(15)	3.3392(3)
b (Å)	11.8093	11.7600	11.7253	4.9297(3)
c (Å)	10.9615(11)	11.0689(7)	11.126(2)	7.4736(5)
α (°)	90	90	90	76.777(5)
β (°)	90	90	90	86.680(6)
γ (°)	120	120	120	78.680(6)
V (Å^3)	1323.9(2)	1325.71(13)	1324.7(4)	117.421(15)
asymmetric unit	C_4 $H_{2.85}$ Li_2 $O_{4.43}$	C_4 $H_{2.44}$ Li_2 $O_{4.22}$	C_4 $H_{2.40}$ Li_2 $O_{4.20}$	C_2 H Li O_2
Z	9	9	9	1
d_{calc} (g cm^{-3})	1.531	1.487	1.484	1.809
μ (mm^{-1})	0.133 (Mo Kα)	0.128 (Mo Kα)	0.128 (Mo Kα)	0.155 (Mo Kα)
reflections collected	1330	2127	1652	3120
unique reflections	936	1273	1067	586
observed data (I > 2σ(I))	696	994	835	558
parameters	107	113	101	49
R_{int}	0.0274	0.0184	0.0209	0.0179
R_1	0.0513	0.0425	0.0847	0.0267
wR_2 (I > 2σ(I))	0.1208	0.1084	0.2339	0.0761
R_1 (all data)	0.0736	0.0588	0.0997	0.0277
wR_2 (all data)	0.1389	0.1236	0.2582	0.0775
GOF	1.069	1.042	1.061	1.107

S2. Comparison of the ^{13}C MAS-NMR spectra of 2(0.77) with hypothetical calculated structures 2(1).

The chemical shifts observed in the experimental MAS-NMR ^{13}C spectra of **1** and **2(0.77)** are assigned in a similar manner to the solution spectra (See main article). Spectra were calculated for the hypothetical structures lithium fumarate (**2(1)**), lithium L-malate (**1**) with 100% occupancy at either the major or minor position (see Table S2 for experimental and calculated chemical shifts). The experimental and calculated values for lithium fumarate are in qualitative agreement, whereby the small differences between carbons with similar chemical environments suggested by the calculations (C1, C4 and C2, C3) are not resolved in the experimental data. As mentioned in the main article, the experimental chemical shifts of lithium L-malate change slightly upon dehydration. Based on the differences between the two hypothetical calculated spectra of **1**, all experimental peaks move in the direction that suggests more of the ligand in the minor site remains. For example, the $\underline{C}H_2$ peak is moved by approximately 1.2 ppm to higher field in **2(0.77)** relative to the corresponding peak in **1**. Calculated spectra of hypothetical **1**, in which the OH group is localized either on the position of major or minor occupancy, indicate that the $\underline{C}H_2$ peak lies at higher field in the latter case. This suggests that there is a preference for the dehydration of the major site, in contradiction with the results of single crystal X-ray diffraction. More extensive calculations, involving several different ligand positions and occupancies within the same cell, that may reflect better the chemical environment of the L-malate ligand in **2(0.77)** were not carried out due to time constraints.

Figure S1. ^{13}C MAS-NMR spectra of 2(0.77) (a) and 1 (b). Inset shows magnification of the CH_2 peak.

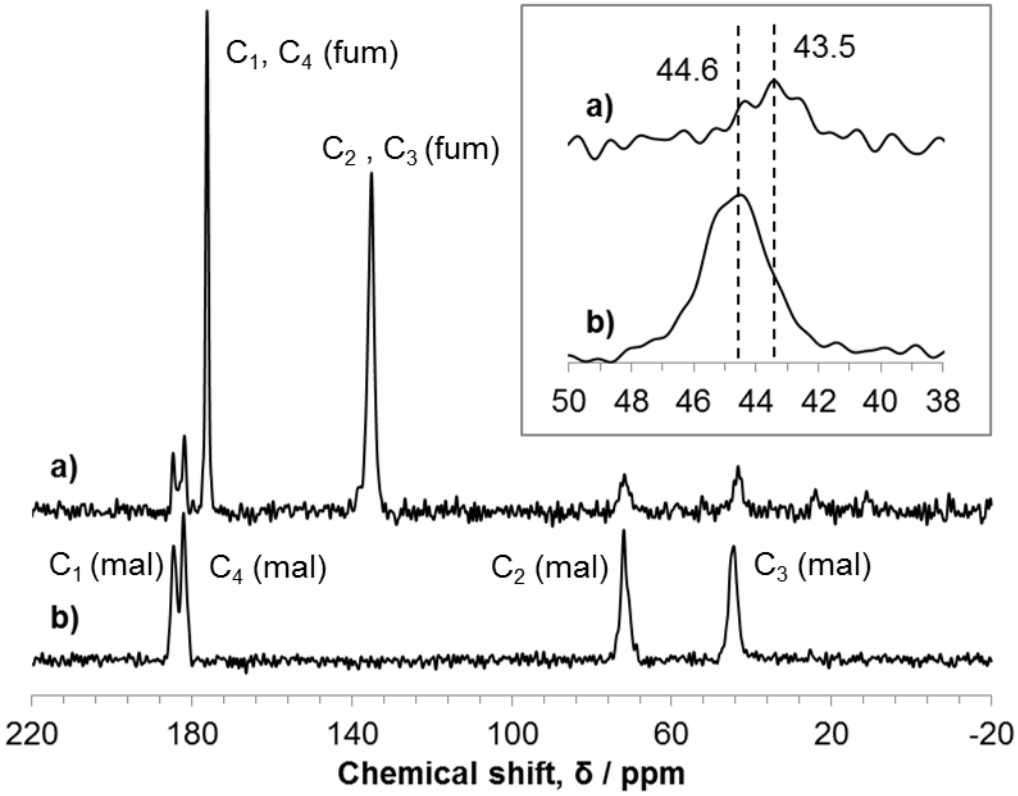

Table S2. Experimental and calculated ^{13}C chemical shifts of L-malate and fumarate ligands in MAS-NMR spectra 2(*x*).

		Experimental (from **2(0.77)**, ppm)		Calculated hypothetical (**2(1)**, ppm)	
Fumarate	C1	176.2		178.24	
	C4	176.2		178.28	
	C2	135.1		139.27	
	C3	135.1		139.65	
		Experimental (from **1**, ppm)	Experimental (from **2(0.77)**, ppm)	Calculated (from **1** assuming full occupancy at major site, ppm)	Calculated (from **1** assuming full occupancy at minor site, ppm)
L-malate	C1 (α- to OH)	184.6	184.7	188.8	189.7
	C4 (β- to OH)	182.1	181.9	184.7	183.8
	C2 (CHOH)	72.0	71.9	74.5	74.2
	C3 (CH_2)	44.6	43.4	43.8	41.4

Figure S2. ^1H NMR spectra of 2(0.77), 3 and 1 (a-c, respectively; D_2O solution). Asterisks mark signals from HOD and unknown impurities.

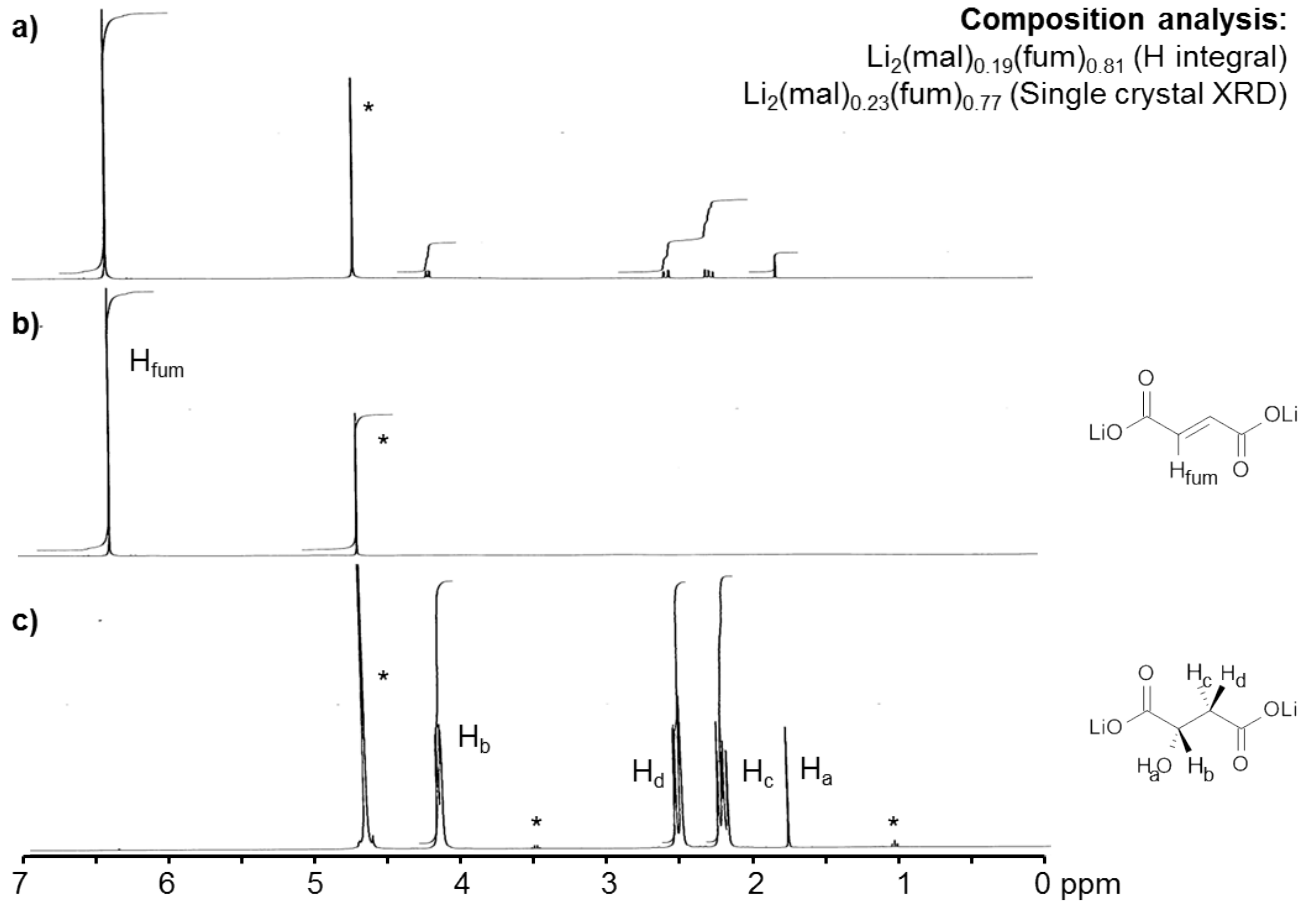

Integration of ^1H peak intensities indicate that x = 0.81, in close agreement to the value obtained by single crystal X-ray diffraction (x = 0.77). Assignments were made as follows (ppm vs. tetramethylsilane, coupling constants (J) quoted in Hz; 500 MHz, D_2O): L-malate δ_H 1.77 (1H, s, OH), 2.20-2.25 (1H, dd, J 10.0 and 15.5, CH_2), 2.51-2.54 (1H, dd, J 3.0 and 15.5, CH_2), 4.14-4.17 (1H, dd, J 3.0 and 10.0, CH); fumarate δ_H 6.37 (1H, s, CH).

Figure S3. ^{13}C NMR spectra of 2(0.77), 3 and 1 (a-c respectively; D_2O solution). Asterisks mark unknown impurities.

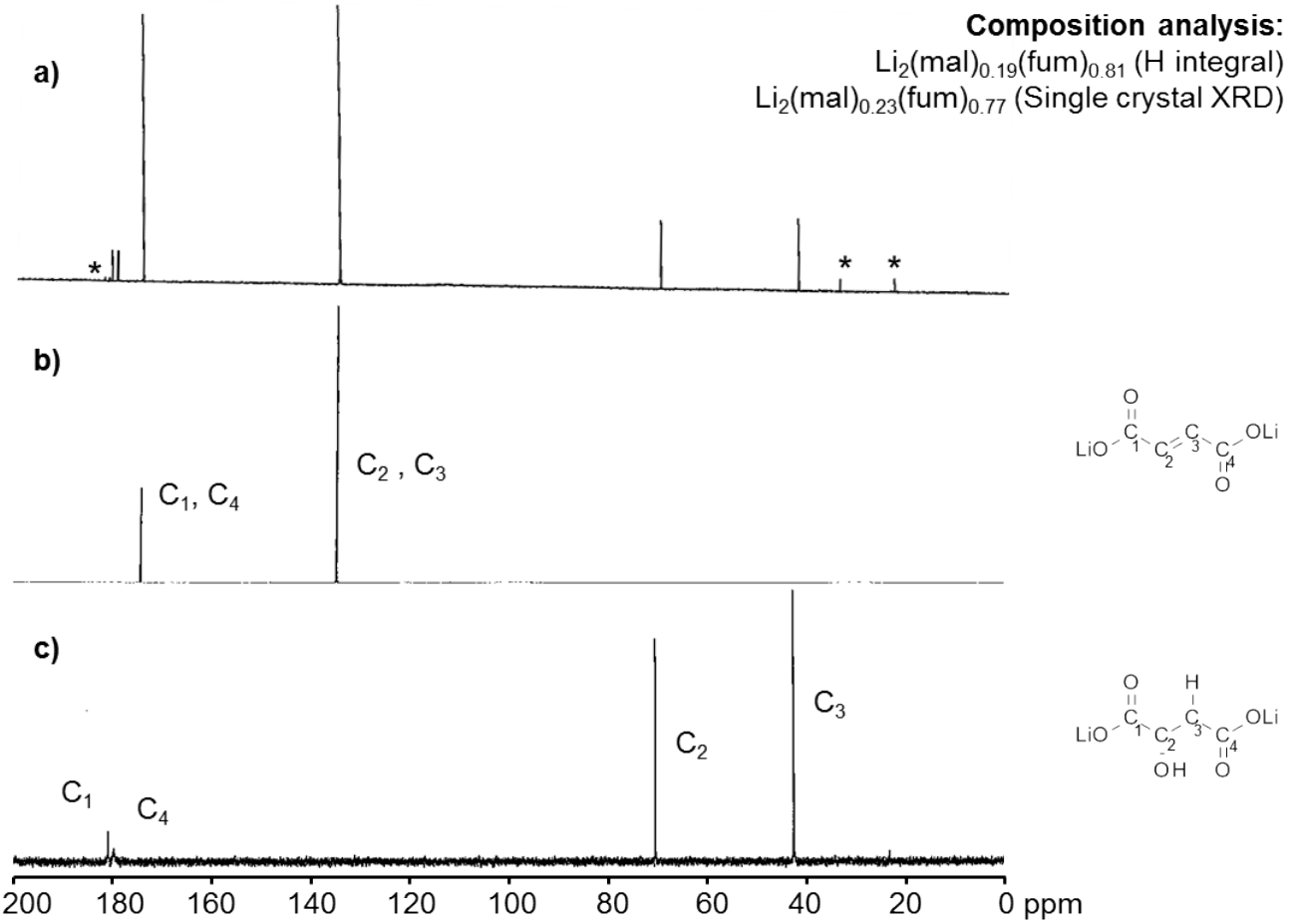

Assignments were made as follows (ppm vs. tetramethylsilane, coupling constants (*J*) quoted in Hz; 500 MHz, D_2O): L-malate δ_C 42.481 ($\underline{C}H_2$), 70.25 ($\underline{C}HOH$), 179.77 ($\underline{C}O_2$-βOH), 180.95 ($\underline{C}O_2$-αOH); fumarate δ_C 135.2 ($\underline{C}H$), 174.63 ($\underline{C}O_2$).

Figure S4. Full FTIR spectra of 2(*x*): a) 1 before heating, b) after 1 hour at 280 °C, c) after 11 hours at 280 °C, and d) after 22 hours at 320 °C. Absorbance is normalized to the carboxylate peak at 1570 cm^{-1}. The gradual loss of the hydroxyl group stretch (3440 cm^{-1}, br) and C-OH stretch (1070 cm^{-1}) and appearance of the *trans*- H-C=C-H out of plane bend (970 cm^{-1}) is observed with increasing time and temperature of reaction. The feature at 2300-2400 cm^{-1} is caused by CO_2 and is an artifact of the background substraction.

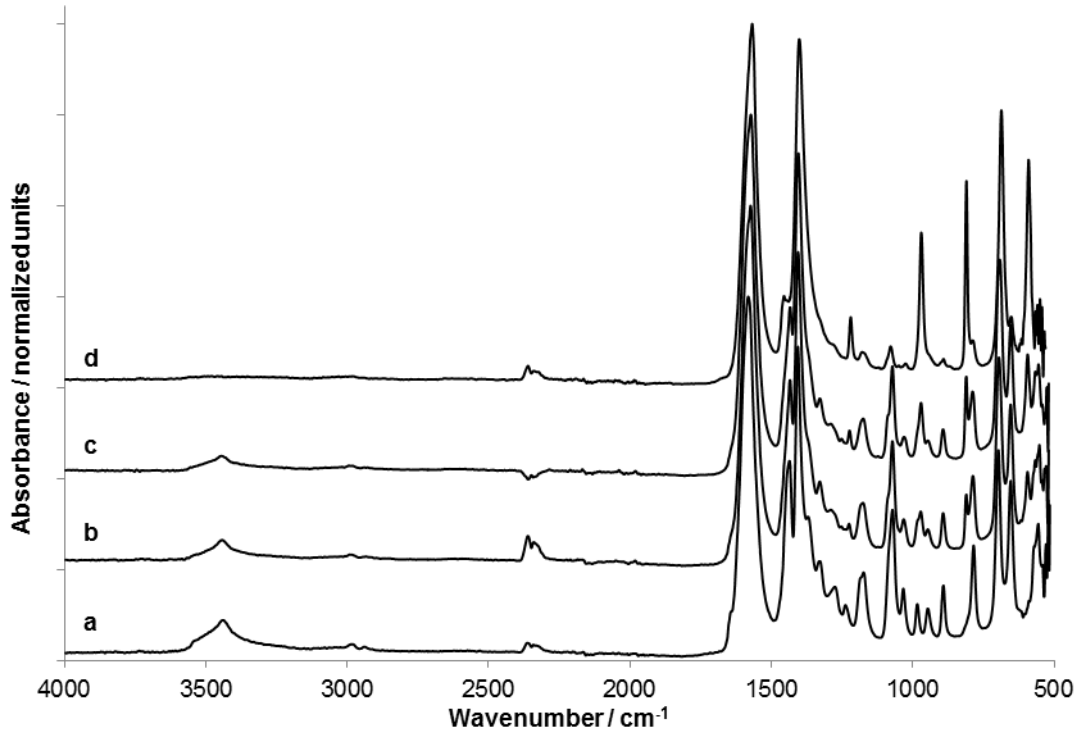

Table S3. Reaction enthalpies calculated using DFT for the hydration of lithium fumarate, comparing PBE, PBE+D2, PBE+D3, *E*+ZPE and *E*+ZPE+E_{vib}(300 K) methods. *x*, Δ*E* and Δ*E'* here only represent the fraction of ligands converted (according to the equation Li_2(fumarate) + *x*(H_2O) → Li_2(fumarate)$_{1-x}$(L-malate)$_x$), the reaction energy per computed cell (9 formula units), and the reaction energy per formula unit, respectively.

	PBE		PBE+D2		PBE+D3		*E*(PBE+D3) + ZPE		*E*(PBE+D3) + ZPE + E_{vib} (300 K)	
x	**Δ*E*** (eV)	**Δ*E'*** (kJ/mol)	**Δ*E*** (eV)	**Δ*E'*** (kJ/mol)	**Δ*E*** (eV)	**Δ*E'*** (kJ/mol)	**Δ*E*** (eV)	**Δ*E'*** (kJ/mol)	**Δ*E*** (eV)	**Δ*E'*** (kJ/mol)
1/9	-0.5	-5.4	-0.7	-7.9	-0.7	-7.6	-0.5	-5.4	-0.5	-5.3
2/9	-1	-11.1	-1.5	-16	-1.4	-15.4	-1.1	-11.8	-1.0	-10.9
3/9	-1.5	-16.5	-2.3	-24.2	-2.1	-23.0	-1.6	-17.2	-1.5	-16.2
4/9	-2.1	-22.3	-3.1	-33.2	-2.9	-31.1	-2.2	-23.6	-2.0	-21.9
5/9	-2.5	-26.8	-3.9	-41.5	-3.5	-37.8	-2.7	-28.9	-2.5	-26.3
6/9	-3	-32.3	-4.7	-50.1	-4.3	-45.8	-3.2	-34.3	-3.0	-32.0
7/9	-3.4	-36.8	-5.5	-58.6	-4.9	-52.5	-3.7	-39.7	-3.4	-36.3
8/9		n/a		n/a	-5.6	-60.6	-4.4	-47.2	-4.1	-44.0
1	-5.5	-58.6	-7.9	-85.1	-7.6	-81.8	-5.9	-63.3	-5.9	-60.3

Figure S5. Visualization of the values shown in Table S3, converted to give energies for progressive dehydration reactions of Li_2(L-malate). Extrapolation of the PBE+D3 data reveals that the energy required to break hydrogen bonding between trimers of hydroxyl groups in 2(0) is 13.7(3) kJ/mol (shown).

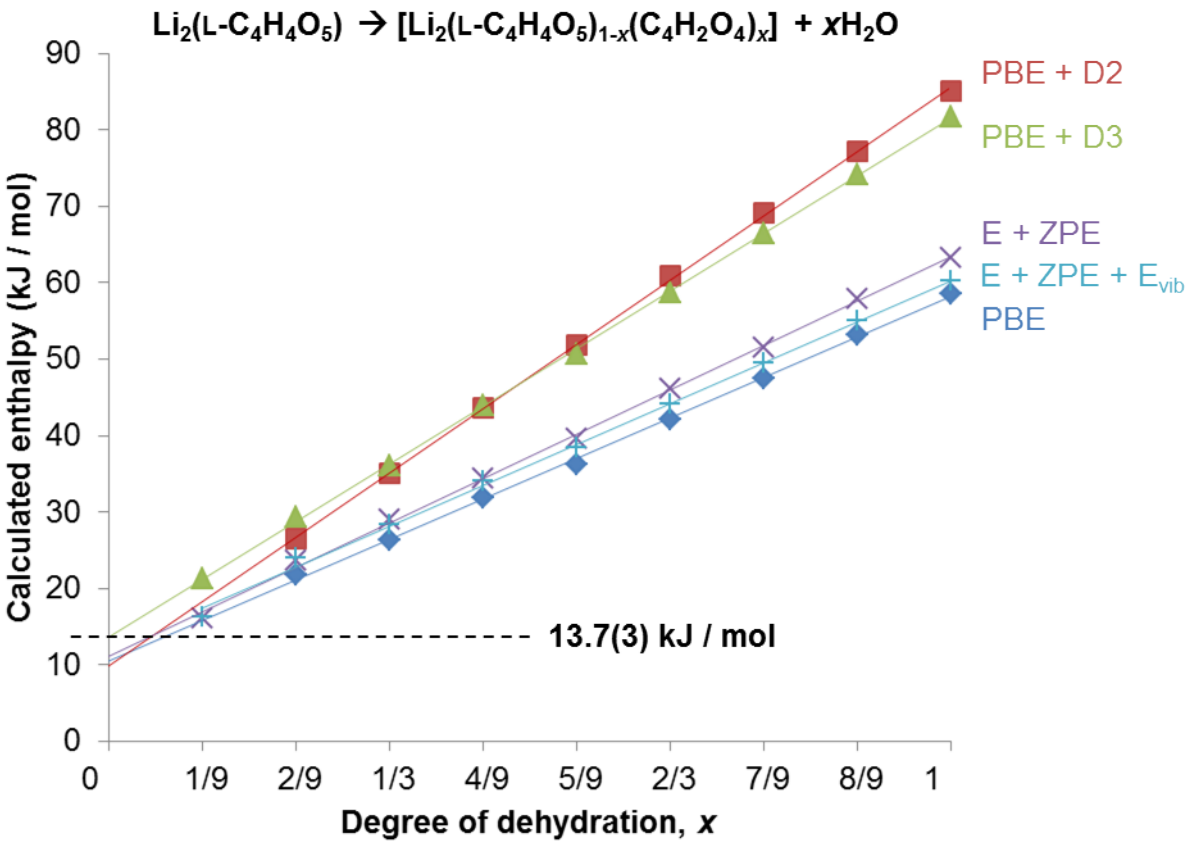

Table S4. Difference in the enthalpies of formation of Li_2(fumarate) polymorphs 2 (hypothetical) and 3 (experimentally observed), comparing PBE, PBE+D2, PBE+D3, *E*+ZPE and *E*+ZPE+E_{vib}(300 K) methods.

	PBE	**PBE+D2**	**PBE+D3**	***E*(PBE+D3) + ZPE**	***E*(PBE+D3) + ZPE + E_{vib} (300 K)**
Enthalpy difference (3-2) (kJ/mol)	9.60	-12.73	-12.89	-12.44	-13.20

Table S5. Tests for accuracy of ZPE with respect to the grid density and step size. Values are given for the computed cell (9 formula units).

	ADDGRID = .TRUE. POTIM = 0.01 ZPE (eV)	**POTIM = 0.015 ZPE, (eV)**
Li_2(L-malate) 1	22.631	22.648
Li_2(fumarate) 2 - hypothetical	15.795	15.792
Li_2(fumarate) 3	15.829	15.831

Figure S6. Variable temperature X-ray diffraction of 2(*x*). Daggers mark peaks from the glassy alumina substrate; asterisks mark Li_2CO_3 peaks.

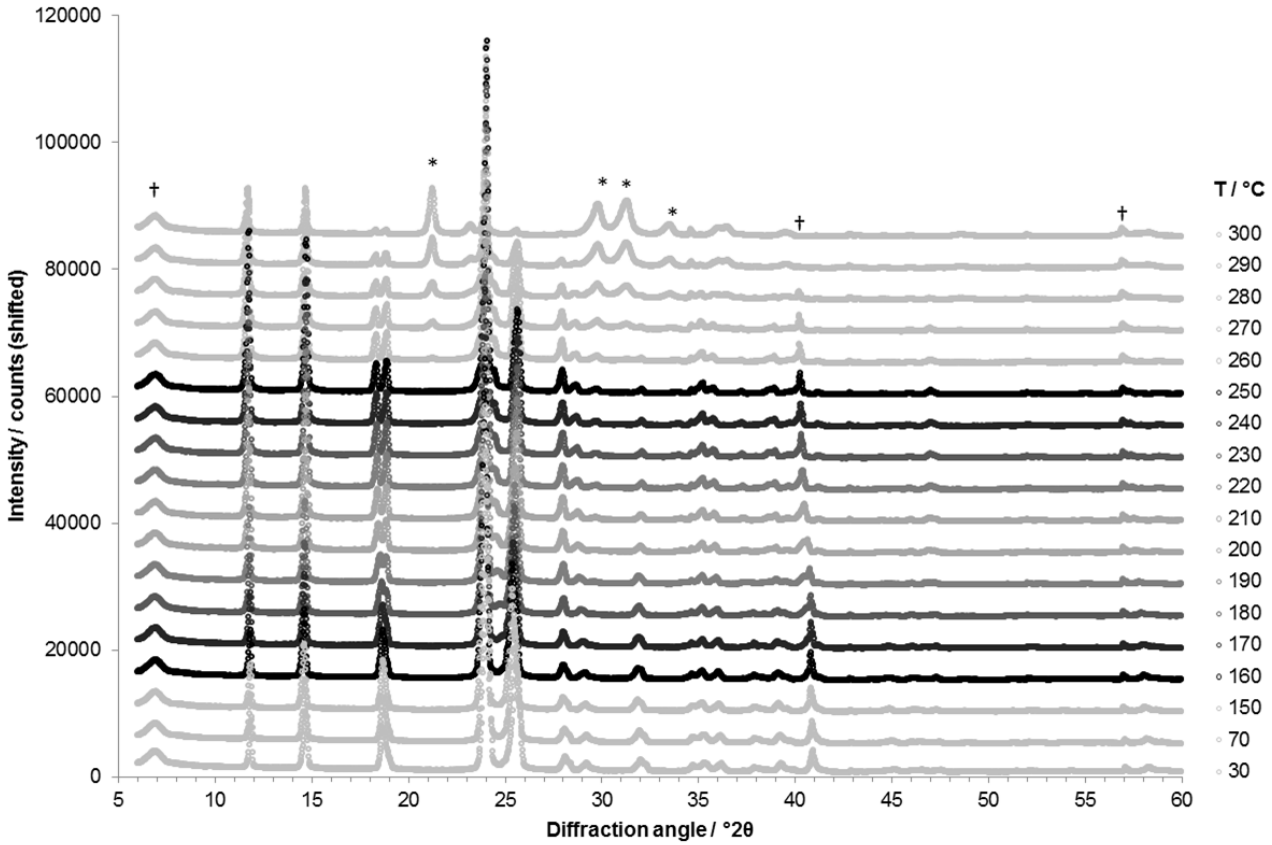

Figure S7. Le Bail refinement of 2(*x*) in *R*-3 using X-ray diffraction data (λ = 1.5418 Å) at $T_{diffraction}$ = 70 °C. Data, model, background and difference curves are shown as blue crosses and green, red and cyan lines, respectively. Tick marks show positions of Bragg reflections.

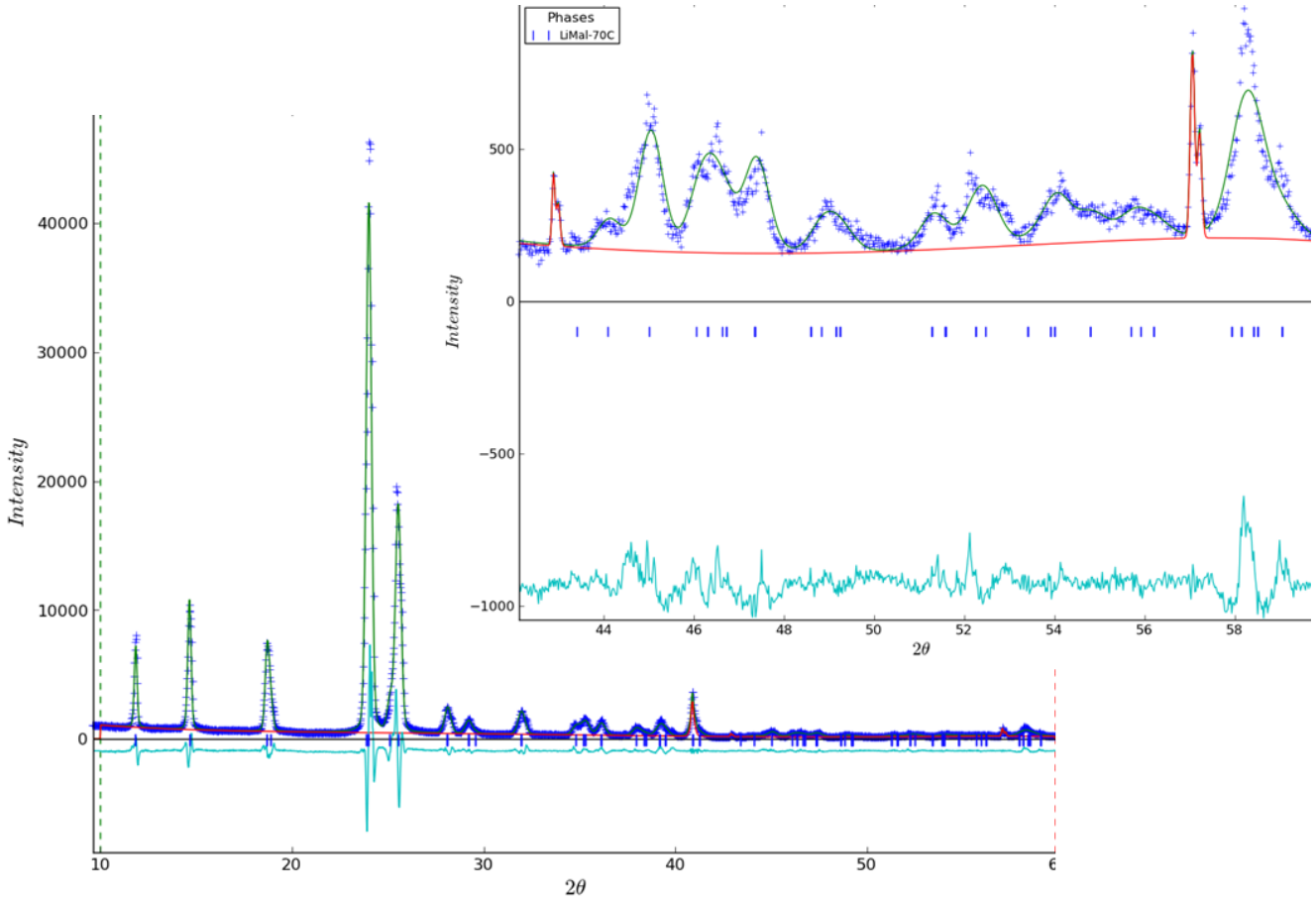

Figure S8. Le Bail refinement of 2(*x*) in *R*-3 using X-ray diffraction data (λ = 1.5418 Å) at $T_{diffraction}$ = 250 °C. Data, model, background and difference curves are shown as blue crosses and green, red and cyan lines, respectively. Tick marks show positions of Bragg reflections.

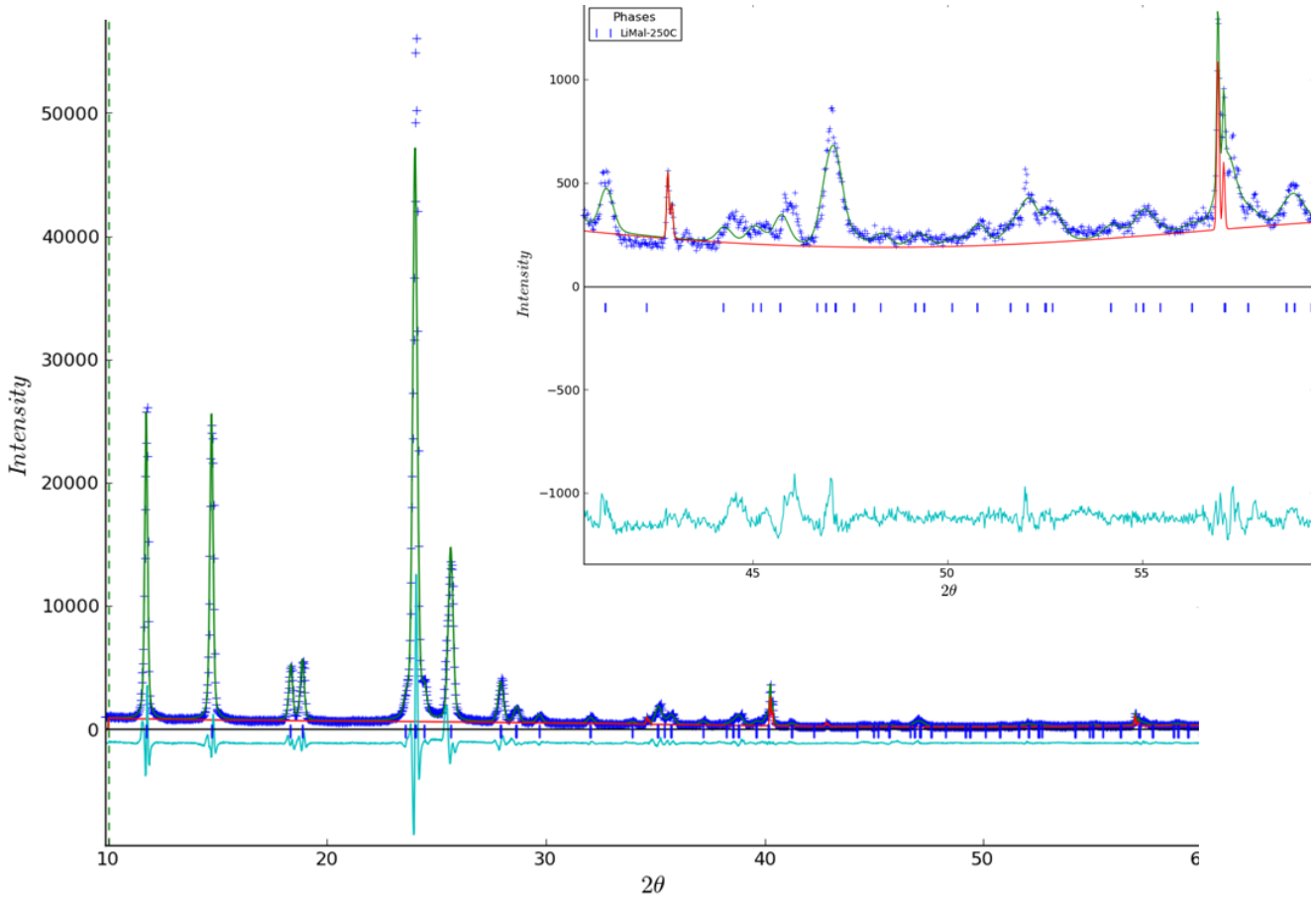

Figure S9. Le Bail refinement of 2(*x*) in *R*-3 and Li_2CO_3 in *C*2/*c* (*a* = 8.475(2) Å, *b* = 4.9868(8) Å, *c* = 6.3278(12) Å, *α* = *γ* = 90°, *β* = 115.28(3)°) using X-ray diffraction data (λ = 1.5418 Å) at $T_{diffraction}$ = 250 °C. Data, model, background and difference curves are shown as blue crosses and green, red and cyan lines, respectively. Tick marks in blue and red show positions of Bragg reflections for 2(*x*) and Li_2CO_3, respectively.

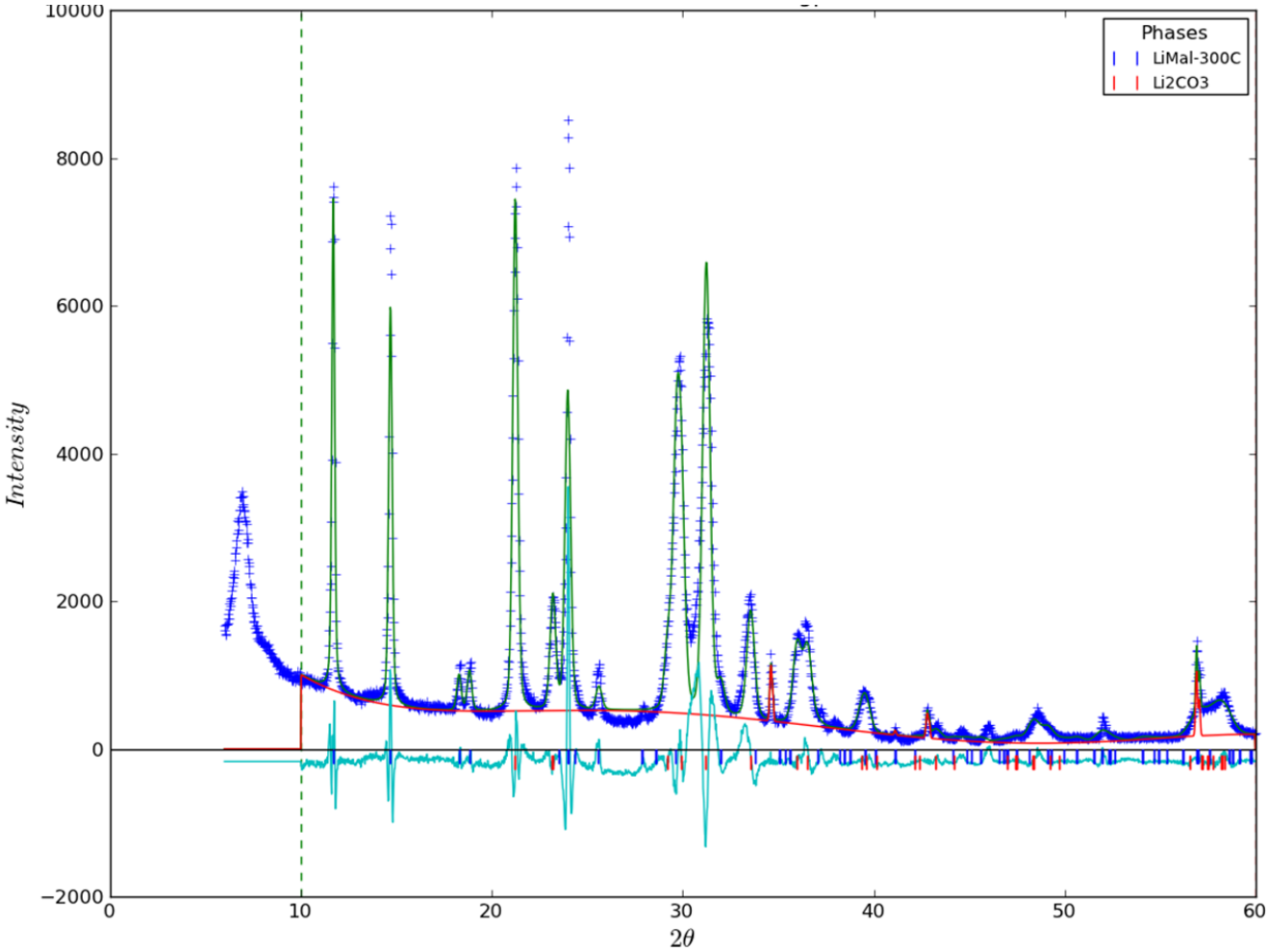

5

Figure S10. Unit cell parameters of 2(*x*) with esd's shown, derived from Le Bail fitting of VT-powder X-ray diffraction data, highlighting processes (i)-(iii) in blue, purple and red, respectively.

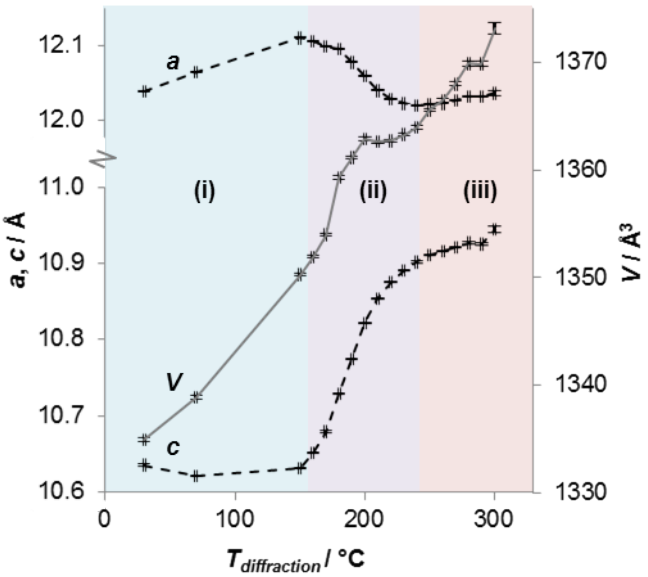

S3. Structural analysis of lithium fumarate, 3.

The extended asymmetric unit of dilithium fumarate, Li_2(fum), consists of half of one fumarate ligand and one lithium atom (Fig. S10). The ligand is planar and retains the *trans* conformation of the conjugated π-system of the starting material. C-C bond lengths are as expected for single and double carbon-carbon bonds, at 1.5002(11) Å and 1.331(2) Å, respectively. The carboxylate oxygen atoms are essentially co-planar with the carbon skeleton, with O1-C1-C2-C2 and O2-C1-C2-C2 torsion angles -8.34(13)° and 169.90(8)°, respectively. The lithium coordination environment is a distorted tetrahedron. Li-O bond distances are remarkably uniform, between 1.942(2) Å and 1.988(2) Å, but O-Li-O angles vary widely between 89.20(7)° and 119.10(8)°. The bond valence sum is 1.02, in good agreement with the expected value for monovalent lithium, although a little lower than most other lithium-based inorganic-organic frameworks. This may be a result of the rigidity of the ligand, which limits the extent to which the LiO_4 tetrahedron can relax.

For the structural comparison of **3** with the hypothetical polymorphic phase **2(1)**, cell parameters and atomic coordinates of the fumarate ligand were taken from the experimentally determined structure **2(0.77)** assuming full occupancy and subtracting the atoms corresponding solely to the l-malate ligand.

The FTIR spectrum of **3** shows many similarities with that of **2(0.77)** (Fig. S11). The topological differences in the structures, along with the presence of L-malate in **2(0.77)** may account for the small differences observed in the positions of several peaks, such as the *trans*-HC=CH out of plane deformation.

Figure S11. Ortep extended asymmetric unit of dilithium fumarate, showing atoms needed to complete one ligand moiety and the lithium coordination sphere. C, H, Li and O atoms are shown in grey, white, green and red, respectively. Additional atoms are labelled in grey.

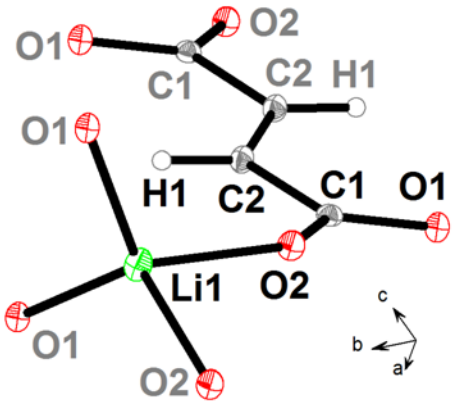

Figure S13. Crystal structure of 3, viewed a) down the *b*-axis, and b) down the *a*-axis, showing ribbons of LiO_4 tetrahedra (green) linked by fumarate ligands (grey) to form a 3-D, I^1O^2 MOF.

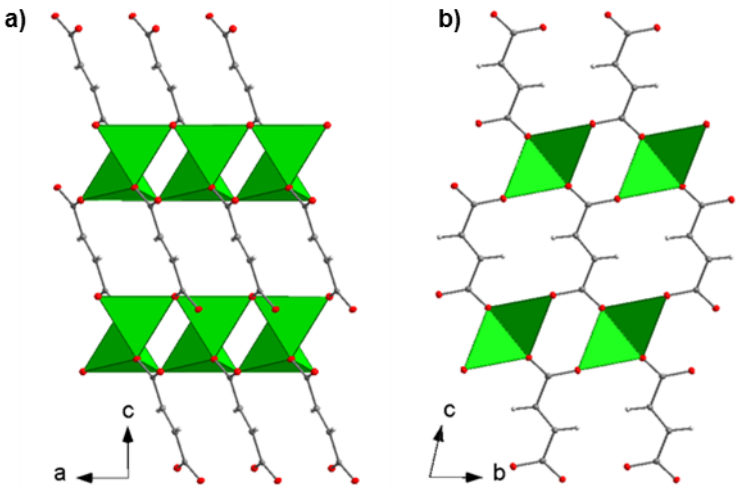

Figure S13. Comparison of FTIR spectra of 3 and 2(0.77).

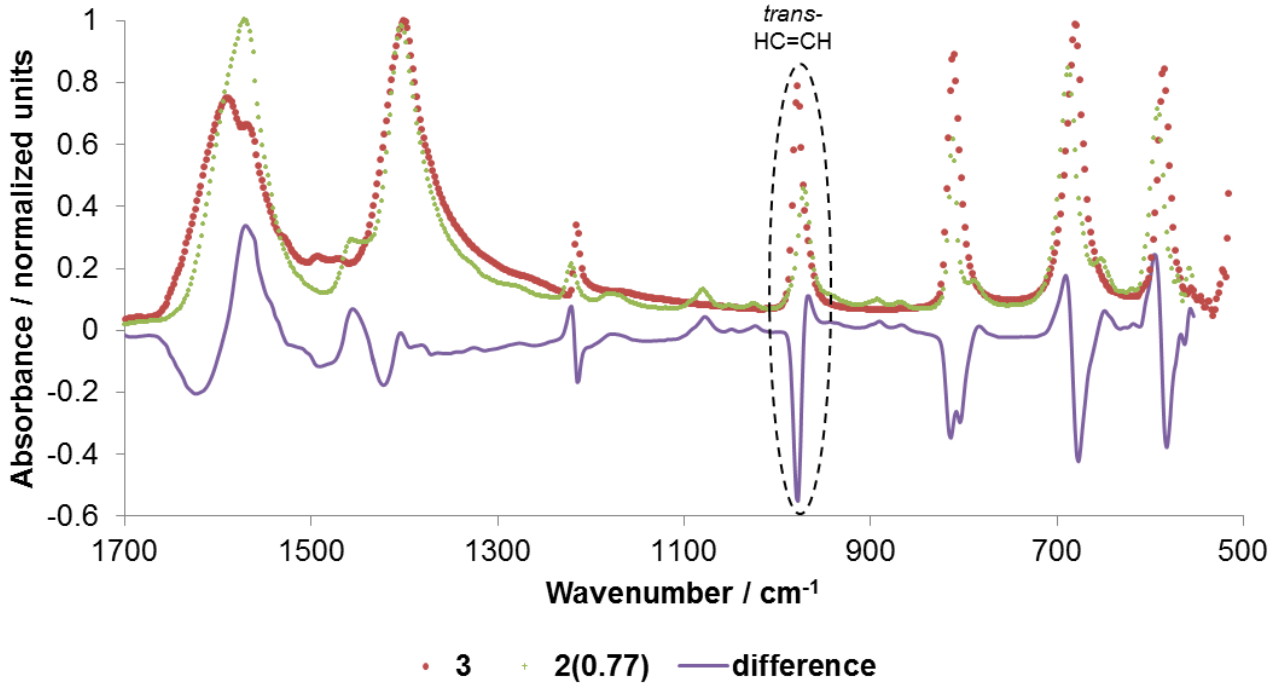

References

1. H. H.-M. Yeung, W. Li, P. J. Saines, T. K. J. Köster, C. P. Grey, and A. K. Cheetham, *Angew. Chem., Int. Ed. Engl.*, 2013, **52**, 5544–7.
2. *CrysAlis CCD, CrysAlis RED and associated programs, Oxford Diffraction Ltd., Abingdon, U.K.*, 2006.
3. G. M. Sheldrick, *Acta Crystallogr. Sect. A Found. Crystallogr.*, 2008, **64**, 112–22.
4. L. J. Farrugia, *J. Appl. Crystallogr.*, 2012, **45**, 849–854.
5. K. Brandenburg and H. Putz, *Diamond 3.2*, CRYSTAL IMPACT GbR, Bonn, Germany, 2009.
6. G. Kresse and J. Hafner, *Phys. Rev. B*, 1993, **47**, 558–561.
7. G. Kresse and J. Hafner, *Phys. Rev. B*, 1994, **49**, 14251–14271.
8. G. Kresse and J. Furthmüller, *Comput. Mater. Sci.*, 1996, **6**, 15–50.
9. G. Kresse and J. Furthmüller, *Phys. Rev. B. Condens. Matter*, 1996, **54**, 11169–11186.
10. P. Blöchl, *Phys. Rev. B*, 1994, **50**, 17953–17979.
11. G. Kresse and D. Joubert, *Phys. Rev. B*, 1999, **59**, 1758–1775.
12. J. Perdew, K. Burke, and M. Ernzerhof, *Phys. Rev. Lett.*, 1996, **77**, 3865–3868.
13. S. Grimme, *J. Comput. Chem.*, 2006, **27**, 1787–1799.
14. S. Grimme, J. Antony, S. Ehrlich, and H. Krieg, *J. Chem. Phys.*, 2010, **132**, 154104.
15. H. H.-M. Yeung, M. Kosa, M. Parrinello, P. M. Forster, and A. K. Cheetham, *Cryst. Growth Des.*, 2011, **11**, 221–230.
16. H. H.-M. Yeung, M. Kosa, M. Parrinello, and A. K. Cheetham, *Cryst. Growth Des.*, 2013, **13**, 3705–3715.
17. S. A. Rivera, D. G. Allis, and B. S. Hudson, 2008, **157**, 10–12.
18. Y. Wang, Y. Zhang, and C. Wolverton, *Phys. Rev. B*, 2013, **88**, 024119.